J Solid State Electrochem (2012) 16:2493–2502
DOI 10.1007/s10008-012-1667-x

ORIGINAL PAPER

On the redox behaviour of glycerol at TiO_2 electrodes

Simonetta Palmas · Anna Da Pozzo · Michele Mascia · Annalisa Vacca · Pier Carlo Ricci · Roberto Matarrese

Received: 14 September 2011 / Revised: 23 January 2012 / Accepted: 25 January 2012 / Published online: 11 February 2012

Abstract An experimental work is presented in which alkaline solutions of glycerol are electrochemically treated at TiO_2 electrodes obtained by electrochemical oxidation of Ti foils annealed a 400 °C and 600 °C. The semiconductor properties of the material, strictly correlated to the presence of structural defects, and their different concentration and distribution originated by the different annealing temperature are investigated. In order to derive useful indications for possible application on reduction or photo-oxidation of glycerol, particular attention is paid on the working mechanism of the electrodes in a wide range of potential at which the semiconductor may be under accumulation or depletion regime.

Keywords Glycerol · Photo-electrocatalysis · Titanium electrochemical oxidation · TiO_2 nanotubes

Introduction

In the last years, the impressive increase of biodiesel production has spread the market availability of glycerol which is obtained in large surplus (e.g. 10% in weight as a by-product) via the transesterification of triglycerides (vegetable and animal oils). As matter of fact, the global glycerol market was 800,000 tons in 2005 with 400,000 tons from biodiesel in comparison to 60,000 tons only in 2001 [1]. As consequence, glycerol is emerging as a flexible bio-feedstock for the production of a variety of chemicals and the development of novel processes able to use it as raw material is of great industrial interest. In this context, a very huge amount of catalytic processes have been proposed for glycerol valorisation [2–4]. A lot of research has been carried out on the oxidation of glycerol to more valuable products and it has been shown that the use of mono- or bi-metallic catalysts based on noble metals (e.g. Au, Pd and Pt) provides tunable selectivity. Accordingly, a complex reaction pathway in which a large number of products such as dihydroxyacetone, glyceric acid, hydroxypyruvic acid, mesooxalic acid and tartronic acid can be produced, which can be used as intermediate compounds for the synthesis of fine chemicals and novel polymers. Another alternative route to exploit glycerol is its hydrogenolysis in the presence of metallic catalysts and hydrogen: propanediols or ethylene glycol can be obtained which at present are industrially produced mainly by using non-renewable sources [5, 6]. Currently, 1,3-propanediol is made by the hydration of acrolein; however, the low conversion efficiency of the acrolein process, as well as its hazardous nature, has spurred a great deal of interest in producing 1,3-propanediol from bio-chemical sources such as glycerol [7].

However, despite the great number of studies and the hopeful results in the development of new catalytic processes for glycerol conversion, many challenges for increasing both selectivity and yield still remain. Besides, concerning the oxidative dehydrogenation, many drawbacks should be solved in the future, such as the low stability of the supported metals in the oxidative environment.

Moreover, from the perspective of green and sustainable chemistry the development of processes based on renewable energy sources, such solar energy, represents the real key issue of the near future in the activation and utilisation of glycerol. As matter of fact a number of opportunities based on photo-

S. Palmas (✉) · A. Da Pozzo · M. Mascia · A. Vacca
Dip. Ingegneria Chimica e Materiali, Università di Cagliari,
piazza D'armi,
09123 Cagliari, Italy
e-mail: spalmas@dicm.unica.it

P. C. Ricci
Dip. di Fisica, Università di Cagliari,
Sestu, Cagliari, Italy

R. Matarrese
Dip. di Energia, Politecnico di Milano,
Piazza L. Da Vinci 32,
20133 Milan, Italy

catalytic and photo-electrocatalytic routes for glycerol consumption have been proposed. As an example, Augugliaro et al. [8] reported the photo-oxidation of glycerol in aqueous suspension in presence of TiO_2 in the anatase and rutile phase for the production of 1-3-dihydroxyacetone, glyceraldehyde and formic acid. Furthermore, recent studies demonstrated the possibility of obtaining hydrogen by photo- or photo-electrocatalytic splitting of water in presence of biomass compounds, such as glycerol [9, 10].

Indeed, nanocrystalline titania is one of the most preferred photo-catalyst material because of its high resistance to corrosion and photo-corrosion in aqueous medium, reactivity to both light and water, cheap and easy availability, environmentally friendly and electronic properties that can be varied by just changing the defect chemistry or oxygen stoichiometry. In addition, several recent studies have indicated that, compared to TiO_2 nanopowders, titania nanotubes have higher surface area, better light adsorption ability and higher photo-catalytic activity [11–16]. In particular, the vertically oriented, immobilised, highly ordered and high-aspect ratio nanotubes may be considered attractive structures for photo-induced processes since they improve the electron transport properties and provide longer electron lifetime, .i.e. by lowering the electron–hole (e-h) recombination which is one of the major practical problems in using TiO_2 as a photo-catalyst.

In this context, an experimental work is here presented in which nanotubular structure obtained by electrochemical anodisation of Ti foils are used to investigate on the redox behaviour of glycerol. In particular, the effect of annealing temperature on both the final structure and the catalytic behaviour of the samples has been investigated. Emphasis is given to the voltammetric study in the potential range at which the space charge of semiconductor structure is in accumulation or in depletion regime. Indication on adsorption at the defective surface, as well as on the redox behaviour of glycerol at the samples is derived.

The use of glycerol as sacrificial reagent in photo-electrochemical cells has been often reported in the literature, not only to minimise e-h recombination losses, but also because it represents an environmentally friendly way to convert it into valuable products [8, 17, 18]. However, in most of the cases the attention was paid on the improvement of electricity or H_2 production. To our knowledge, the present work may represent a first attempt to focus on the redox reaction mechanism of glycerol at TiO_2 nanotubular structures.

Experimental section

Preparation of the electrodes

A sample 4×2 cm^2 of Ti (0.25 mm thick, 99.7% metal basis, Aldrich) was used as starting material to obtain the TiO_2 electrodes. According to a previously reported procedure [19], after a preliminary degreasing treatment the Ti foil was electrochemically oxidised at 20 V in 0.4 M NH_4NO_3+ 0.25 M NaF. Three samples 1×2 cm^2 were then cut from the initial foil: two of them were submitted to different annealing treatment in order to transform the amorphous into crystalline structure: R400, annealed 3 h at 400 °C; R600, annealed 3 h at 600 °C. All the annealing treatments were performed in air. The last sample, RA, was maintained amorphous. Also some samples were prepared in anodisation solution which did not contain fluoride ions, in order to obtain compact oxide layers, we used as comparison. Compact layer samples (RC) were submitted to the same annealing procedures adopted for nanotubular samples.

Raman analysis indicated that anatase phase was generally present in the sample treated at 400 °C (Fig. 1a) while percentages of rutile were found in those treated at 600 °C (Fig. 1).

Micro-Raman measurements have been carried out in back-scattering geometry by using the polarised 514.5 nm line of an Argon ion laser. Raman scattering measurements have been performed in air at room temperature with a triple spectrometer Jobin-Yvonne Dilor integrated system with a spectral resolution of about 1 cm^{-1}. Spectra have been recorded in the Stokes region by a 1,200 grooves/mm grating monochromator and CCD detector system. Confocal microscope Olympus B-201 has been used, with an objective ×100 with 0.90 numerical aperture. The spatial resolution was less than 1 μm. In order to verify the homogeneity of the samples and the reproducibility of the reported data, all the measurements have been repeated in different random points of the samples.

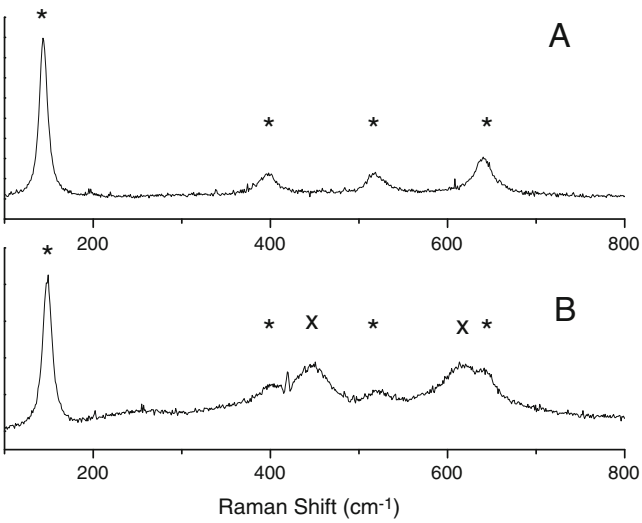

Fig. 1 Example of Raman spectra of samples annealed at 400 °C (**a**) and 600 °C (**b**). Symbol (*) indicates the main anatase bands, while symbol (x) indicates the vibrations associated to the rutile phase

Scanning electron microscopy (SEM) was used to study the morphology of the assembled electrodes. SEM measurements were performed with a NovaNanoLab 600 (FEI) working in the high vacuum mode (accelerating voltage 2 kV).

Figure 2 shows the SEM images, at two different magnifications, of the sample treated at 400 °C. No appreciable difference in the morphology with the annealing temperature was detected by SEM analysis.

The electrochemical cell

A three-electrode cell was used for the electrochemical runs, in which the TiO_2 sample was the working electrode: for all the experiments its surface was shielded so that a nominal area of 1 cm^2 was exposed to the electrolyte. A platinum grid and a saturated calomel electrode (SCE) constituted the counter and the reference electrodes, respectively; all the values of potential in the text are referred to SCE.

Experimental runs

Electrochemical impedance spectroscopy measurements were performed at different bias potentials for each sample, in order to investigate on the capacitance of the semiconductor/electrolyte interphase. Tests were performed in KOH (0.1 M) electrolyte. A frequency response analyzer (FRA, Model 7200 AMEL) was used to perform these experiments in a frequency range from 100 kHz to 0.1 Hz. The Mott–Schottky (MS) analysis was performed in which the imaginary part of the impedance was used to derive the capacity values at the different potentials.

Polarisation curves were obtained in the dark or under irradiation by imposing a potential ramp from the open circuit voltage (OCV) to about 1.5 V with a scan rate of 5 mV s^{-1}. Photo-currents were calculated in KOH or in the presence of glycerol (G), by subtracting the values obtained in the dark from those measured under radiation.

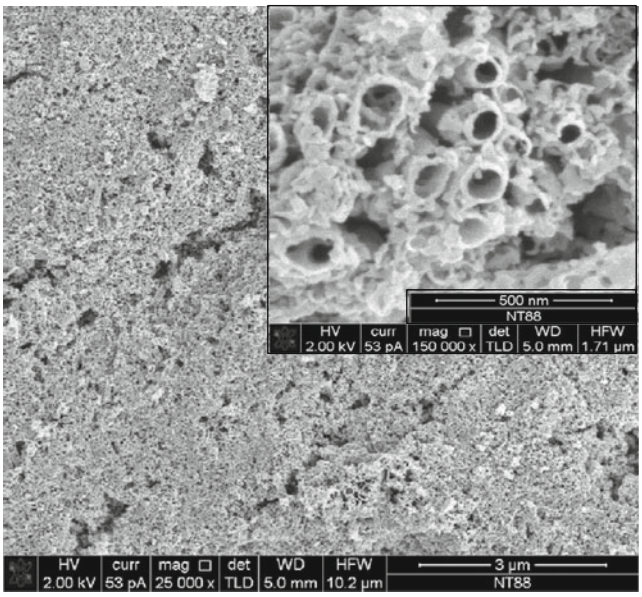

Fig. 2 SEM images of the sample R400

The light source was a 300-W Xe lamp (Lot Oriel): all the photo-experiments presented were carried out with a 365-nm wavelength filter. The average light intensity striking on the surface of the electrodes was about 1.3 mW cm^{-2}.

Cyclic voltammetric (CV) runs were performed in KOH (0.1 M) electrolyte. Two voltammetric scans were repeated: the first one started from the OCV towards the negative potential down to −1.5 V, then backwards to 2.5 V and again to −1.5 V. The scan rate was 200 mV s^{-1}.

The same CV runs were repeated in the presence of 0.1 M glycerol both in the dark and under light irradiation. The effect of the adsorption of G was particularly investigated by performing different CV runs after that samples were maintained in contact with 0.1 M G solution for increasing intervals of time. For all the runs chemicals were of reagent grade (supplied by Aldrich) and they were used as received.

Results and discussion

The electrode structure

Nanotubular structures of TiO_2 were obtained by electrochemical anodisation of Ti foils performed in aqueous solutions containing fluorides. This kind of structures, already used in our laboratory to catalyse the photo-electrosplitting of water [10, 19], guarantee high specific area and high effectiveness in exploiting the light, when used as photoanodes. Depending on the operative conditions adopted in the fabrication of the nanostructures, photo-currents up to 20 times higher than those measured at compact TiO_2 films were obtained [10]. As it will be shown later, under the conditions adopted in the present work, ratios of at least 7 and 10 between photo-currents at nanotubular and compact electrodes was measured in KOH solution, and in the presence of G, respectively.

Defects originated during the formation of the oxide structure play an important role in determining the electro-photo-activity of the sample. Indeed, the oxide film originating from the Ti substrate is oxygen deficient: its structure is generally indicated as TiO_{2-x}. Oxygen ion vacancies, which in their nature are donors, confer a n-type semiconductor behaviour, and represent the dominant Schottky point defects in the resulting structure of the sample. Actually, one missing surface oxygen atom results in two adjacent Ti^{3+} sites [20]. Depending on the ionisation, their energetic levels may be more or less near to the conduction band edge, and in turn their involvement in the activity of the sample more or less favoured: the neutral oxygen vacancy rather easily

donates an electron to become a single charge oxygen vacancy. Deep donor levels in the band gap result from the second ionisation [21].

Mott–Schottky analysis allowed investigating on the electronic structure and on the possible distribution of the energetic levels in the gap. Actually, the MS analysis allows evaluating both flat band potential (E_{fb}) and donor concentration (N_D) that in undoped TiO_2 represents well the concentration of oxygen vacancies (V_O) [22].

Based on this analysis, the space charge capacity has been calculated from the imaginary component of impedance z'' (in the present case measured in the range of 10^5 to 0.1 Hz) as $C_{sc}=1/(2\pi fz'')$. Actually, the capacity should linearly vary with the potential, according to the following equation:

$$\frac{1}{C_{SC}^2}=\frac{2}{\varepsilon_r\varepsilon_0 qN_D}\left(\left(E_{appl}-E_{fb}\right)-\frac{kT}{q}\right) \quad (1)$$

were k is the Boltzmann constant, T the absolute temperature, q the electron charge, ε_0 the vacuum dielectric constant and ε_r the relative dielectric constant of TiO_2.

Figure 3 presents the results from the MS analysis performed at the two annealed samples R400 (a) and R600 (b). As it can be seen, a strong variation of data with the frequency is obtained just indicating the presence of intragap states [23]. At each applied potential value, the further the energetic level of the state from the conduction band edge, the slower the rate of its trapping/detrapping process: the effect of the deepest, and in turn slowest states, is then perceived only at the lowest frequencies [22].

As a result, by decreasing the frequency, a higher number of defects is involved in the capacitive process. Consequently, the value of N_D increases and a flat band potential value less negative is calculated from the intercept to the x axis. Such a value is indicated as apparent flat band potential (E_{fb}*) in Table 1: as an example the values of N_D and E_{fb}* calculated at three different frequencies are reported.

Of note, the two samples show very different values of E_{fb}* and N_D, frequency being the same: the great effect of the annealing temperature confirms that during the oxidation of Ti a high concentration of superficial defects was originated, which are very sensitive to the thermal effect. For this reason at R600, at which defects are present in a lesser extent, a lower value of E_{fb}* is calculated, which is very similar to that expected for titania oxide at this pH values (−1 V vs SCE) [24].

Analogous information is obtained from the voltammetric behaviour of the electrodes in KOH aqueous solution. Figure 4 depicts a comparison between the trends of the CVs for samples annealed at different temperature: for each sample the first and the second scans are shown. The different area involved in the CV confirms the decrease in the

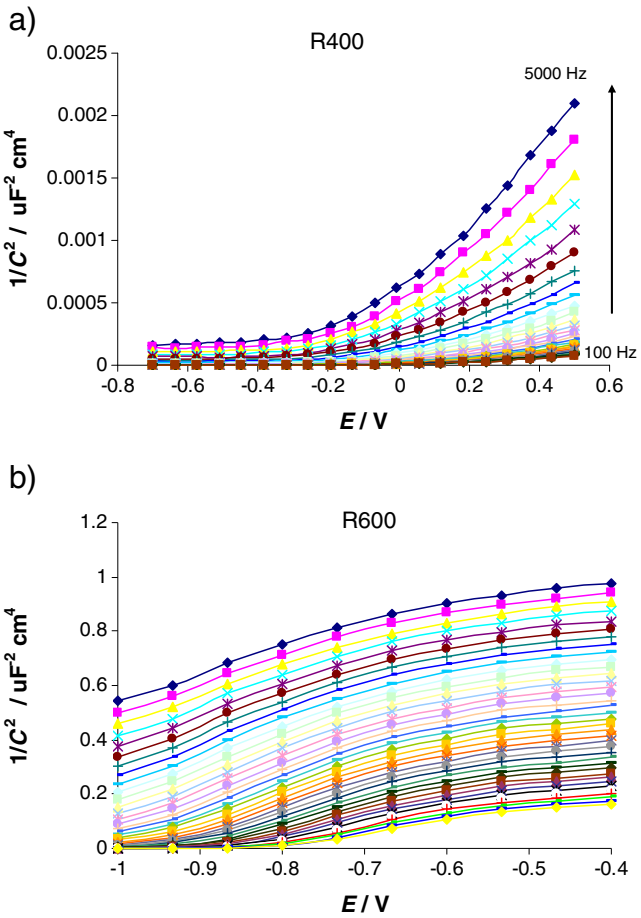

Fig. 3 Effect of the frequency on the Mott–Schottky plot measured at R400 and R600 samples

capacity of the sample annealed at higher temperature, already observed with the MS analysis.

Also the nature of the superficial terminations of the two samples seems to be different: changes in TiO_2 surface state during the annealing process can lead to significant changes in the water absorption properties of TiO_2, because of the possible water loss connected to the thermal treatment, but also because of the phase transition anatase-to-rutile, which can modify the nature of the interactions of the surfaces with water. Thus, the high increase in the current observed at R400 at potential greater than 1.5 V, may indicate the presence

Table 1 N_D and E_{fb}* values obtained at 100, 1,000 and 3,000 Hz for the investigated electrodes

	R400		R600	
Freq (Hz)	N_D (cm^{-3})	E_{fb}* (V)	N_D (cm^{-3})	E_{fb}* (V)
3,000	2.2×10^{21}	−0.2	3.1×10^{18}	−1.2
1,000	6.7×10^{21}	−0.1	2.9×10^{18}	−1.11
100	3.3×10^{22}	+0.06	4.8×10^{18}	−0.90

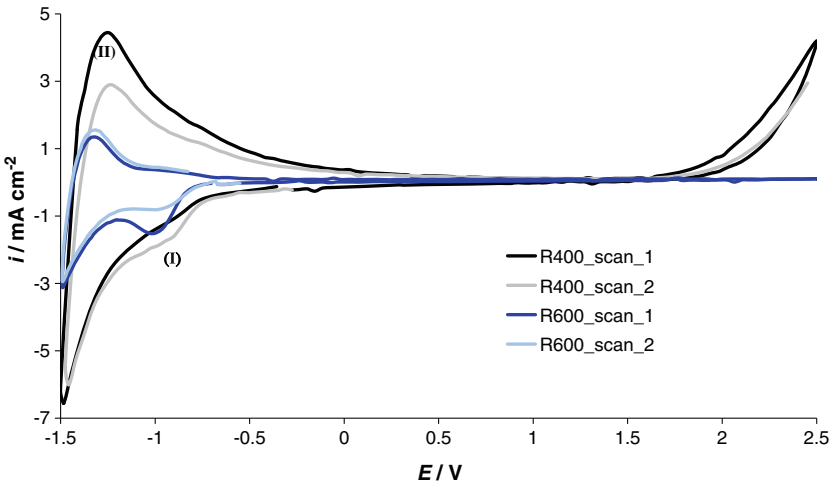

Fig. 4 Comparison between two consecutive voltammetric scans performed in 0.1 M KOH at R400 and R600

of OH terminations favourable to the oxygen evolution, while a higher oxygen overpotential is observed at R600.

If the first scans of the CV are compared, at both the samples a reduction peak (I) is more or less evidenced at about −1 V which can be attributed to quasi reversible redox Ti^{+4}/Ti^{+3} couple [25]. The negative current recorded at this potential can be correlated to the injection of electrons in the oxygen vacancies ($Ti^{+4}+e^{-}\rightarrow Ti^{+3}$). At more negative potential the reduction of the solvent and the incorporation of H in the lattice is recorded.

A significant difference between the trends of two consecutive reduction scans is worth to be considered: at R400, after the sample was submitted to oxidative potential in the first scan, the current measured at the cathodic peak (I) increased: due to the high oxidation current measured at high positive potential (E>1.5 V), oxygen may be restored in the structure which results in a higher concentration of Ti^{+4} sites.

Different behaviour is observed at R600 where a decrease in the peak (I) is measured in the second scan: the absence of O_2 evolution current at high potential, may be the reason of the lack of restoring of the previously reduced sites.

A different strength of the sites at the two samples in bonding the H, may also be the reason for the differences in the anodic current of H oxidation (peak II), measured during the second scan in the two samples. No appreciable difference is noticed between currents recorded at peak (II) during two consecutive scans at R600, indicating a reversible redox process, while the lower current measured during the second scan at R400, may indicate that at this sample H is strongly bonded to the sites.

Redox behaviour of glycerol

Raman analyses performed at amorphous and crystalline samples (Fig. 5), after they were immersed in 0.1 M G solution for 2 h, and then carefully rinsed in distilled water, indicated that the crystalline structure is needed in order to adsorb the organic: an evident peak related to the vibration of the C–H bond was revealed at crystalline anatase, while it was absent at the TiO_2 amorphous sample. Same indication arises from data in Fig. 6 in which no appreciable difference is noticed among the voltammetric scans performed in KOH or in the presence of G when RA sample is considered. Different results were obtained with the crystallised samples, as can be seen from Fig. 7, where the trend of the initial scan of the CV, for R400 and R600, is reported: each curve is obtained after the samples were maintained in contact with G alkaline solution for increasing intervals of time. For both R400 and R600 samples a cathodic peak is observed at −1.1 V, the height of which increases with time of contact with glycerol indicating a slow adsorption process: about 20 h seem to be needed to saturate the sample surface. Actually, if we observe the trend of the peak (I) in the second CV scan (Fig. 8), in both the samples the curves

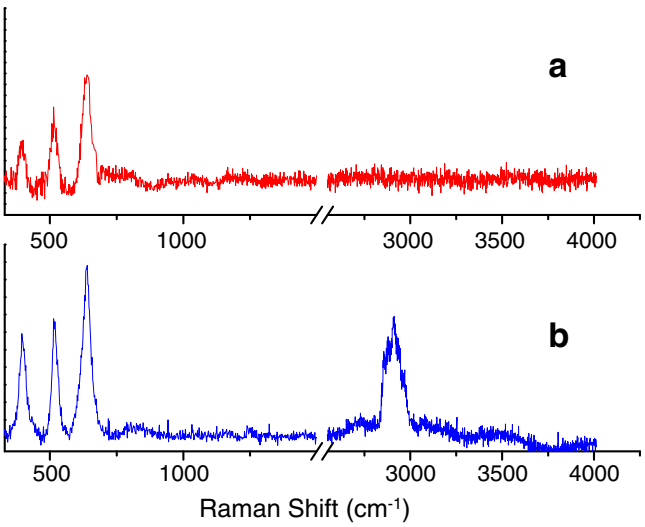

Fig. 5 Comparison between Raman spectra at amorphous (**a**) and crystalline sample (**b**) after they were contacted with G solution for 2 h

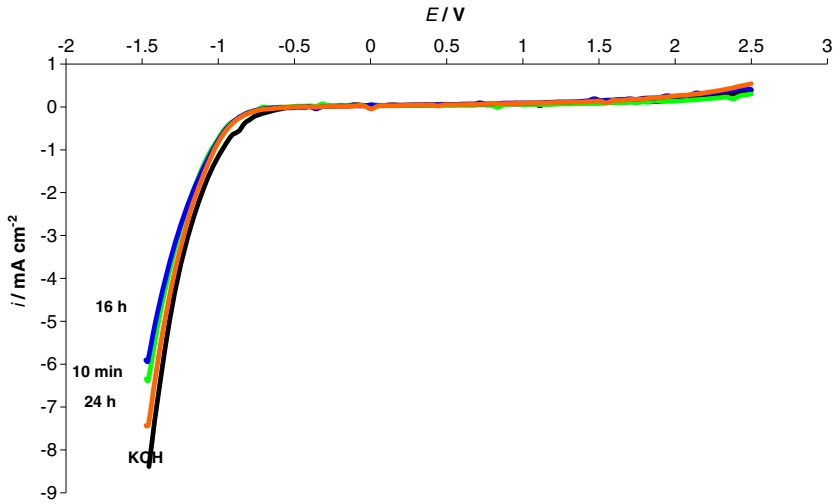

Fig. 6 Effect of G adsorption on the first reductive voltammetric scan performed at RA: each curve is obtained after the sample was maintained in contact with [G]=0.1 M alkaline solution for increasing intervals of time *t*. *Black curve* refers to run performed in the solvent without G

tend to be overlapped to those related to the solvent. This trend can be justified considering that during the first scan G adsorbed inside the tubes may be reduced; however, during the second scan, the high scan rate of the voltammetric run, along with the low diffusion rate of G, lead to a strong decrease of the concentration of G within the tubes, which in turn results in a decreasing of the measured reduction current.

Indication about the reduction mechanism of G can be also argued by the trend of currents measured at peak (II) at the most negative potential (Fig. 8). Actually, by comparing the trends of CV recorded in presence or in absence of G, we can

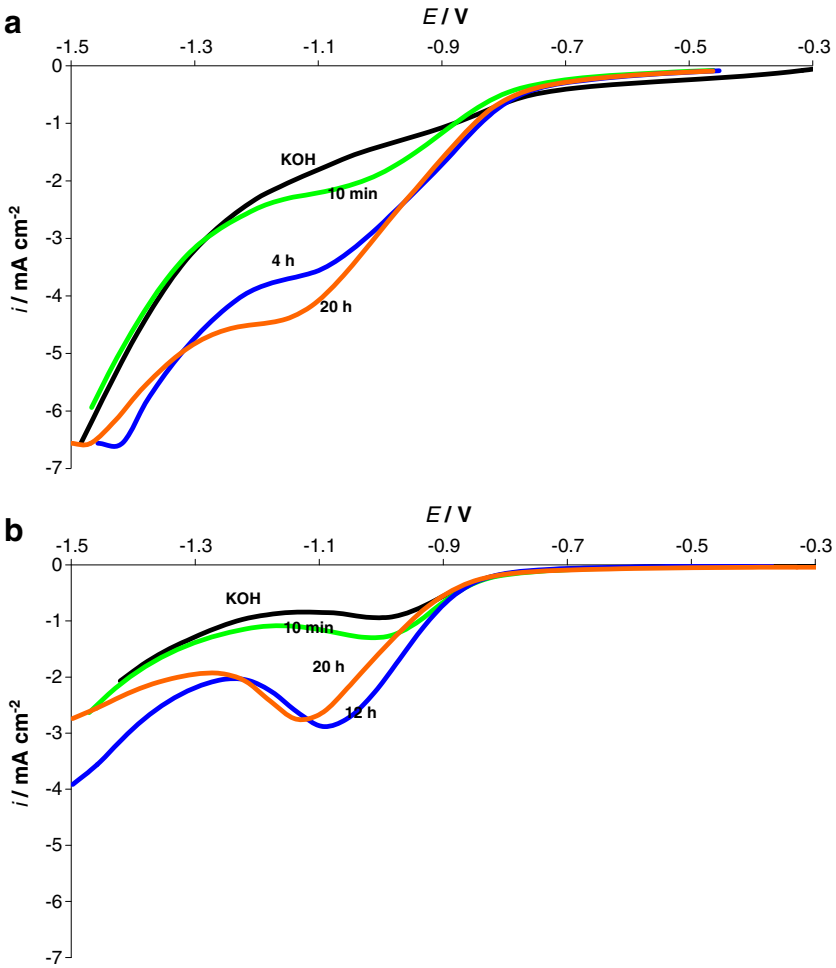

Fig. 7 Effect of G adsorption on the first reductive voltammetric scan performed at R400 (**a**) and R600 (**b**): each curve is obtained after the sample was maintained in contact with [G]=0.1 M alkaline solution for increasing intervals of time *t*. *Black curve* refers to run performed in the solvent without G

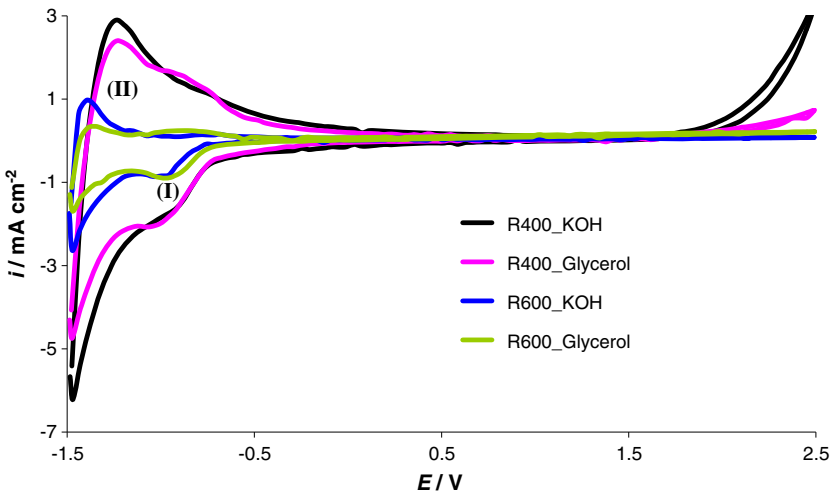

Fig. 8 Cyclic voltammograms for sample R400 and R600 in KOH 0.1 M in absence and in presence of 0.1 M glycerol

observe that at R600, the presence of G in the solution depletes the current at peak (II) by 64%, while the same peak decreases by only 17% at R400 sample. The different phase composition of the two samples, along with their different thermal treatment, may be responsible for the different observed behaviour. Actually, at R400, mainly constituted by anatase, a high density of oxygen vacancies or more superficial defects is present, at which the dissociative adsorption of water leads to a high density of OH terminations [26, 27].

A direct reduction mechanism of G may be thought at R400 at which G replaces the OH terminations of the surface and reacts directly with the injected electrons: accordingly, in the presence of G, a strong decrease in the oxygen evolution current at $E>1.5$ V is measured at this sample.

On the contrary, at R600, a weaker adsorption of molecular water is likely to be favoured: due to both the decrease in defects caused by the thermal effect and to the presence of a certain percentage of rutile detected at this sample, a lower amount of water may be adsorbed [28, 29]. Thus, unlikely from the previous sample, a lower concentration of OH termination is available to be replaced by G. An indirect reduction mechanism may be hypothesised in this case: the lower current recorded at the peak (II), may indicate that in this case the adsorbed G is reduced by H incorporated in the lattice.

Behaviour under UV irradiation

In order to exploit the semiconducting character of TiO_2 the behaviour of the electrodes has to be considered under depletion conditions, that means at potential more positive than the flat band potential. In this range of potential no current is measured in the dark due to the depleted state of the space charge of the semiconductor. However, as it is well-known, when a semiconductor is irradiated by a light with a sufficient wavelength, photo-current is obtained due to the photo-generated electrons and holes. If the electric field is high enough the photo-generated charges may be effectively separated: while the holes are scavenged by the electrolyte, the electrons can move through the film and will have two functions: first they fill up part of the available traps and second, they can react with electron acceptors in the electrolyte. In the present case an electrically enhanced process is thought in which an external bias potential is applied contemporary to the light irradiation, which helps the electric field in the space charge to be maintained, so that recombination of the charges is avoided or limited.

Figure 9 shows the results of photo-current tests performed at both the samples in alkaline G solution and in the solvent. Also data obtained at compact oxide electrode are enclosed in the same graph as a comparison. Photo-currents measured at the quasi stationary state in the range of potential higher than the flat band potential values, are plotted in terms of values normalised with respect to the incident power of the light. Photo-electrosplitting of water is evident from the polarisation curves performed in KOH at R400 and R600 samples. Also we can note that the potential on set of photo-currents is almost the same at the two samples and that, in both the cases the presence of G in the electrolyte increases photo-currents (blue curves): due to the high hole scavenger character of G, recombination of the charges is hindered.

Although photo-activity is worth to be considered in the depletion regime, the behaviour of the system in the accumulation regime can give useful information on the understanding of the full catalytic process. Thus, Fig. 10 depicts the comparison between CVs obtained at the two samples, in KOH and in the presence of G, when they were submitted to the light irradiation at a wavelength of 365 nm. The range of potential more negative than the flat band potential is also reported in the graph. For both the samples, an increase in the cathodic peak (I) is measured during irradiation in KOH, which is attributable to an increased number of Ti^{+4} sites

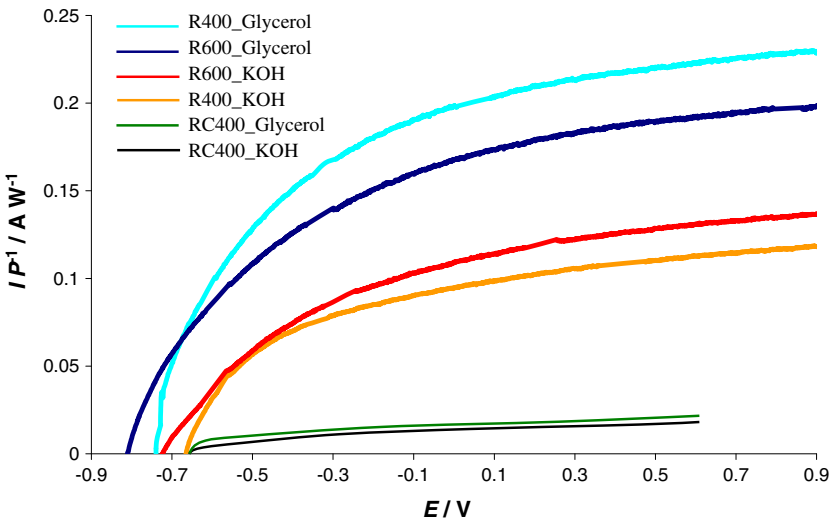

Fig. 9 Trends of photo-current (normalised to incident power light) vs potential, for the investigated samples, in KOH 0.1 M in absence and in presence of 0.1 M glycerol. λ= 365 nm

which are restored by the photo-generated holes. The presence of G in the solution (symbols in the Fig. 10) depletes the current measured at the peak (I) because G blocks the access to the superficial sites which mediate the interface charge transfer. The lower concentration of superficial sites at R600 could be evoked to justify the higher percentage of decrease in the current, the amount of G which has contacted the samples being the same.

Some considerations can be drawn, on the basis of the experimental results of this work:

- The catalytic substrate is constituted by TiO_2, at which by the effect of different annealing temperature, different concentration of defects are originated mainly constituted by oxygen vacancies V_O.
- Samples annealed at 400 °C have shown higher concentration of V_O, which in turn results in higher concentration of OH terminations, since they preferentially adsorb at the V_O. As a consequence, the oxygen evolution reaction at R400 is favoured. The O_2 evolved restores the oxygen in the lattice, so increasing the concentration of Ti^{+4}; thus the current recorded at the reduction peak (I) related to Ti^{+4}/Ti^{+3} shows an increase in the second cathodic scan.
- At samples annealed at 600 °C the concentration of V_O is lower due to the higher temperature adopted in the thermal treatment; so the absence of OH terminations at the surface causes an increase in the overpotential for oxygen evolution. In this case the oxidative scan is not able to restore Ti^{+4} and the voltammetric peak related to its reduction does not increase in the second cathodic scan.
- Under the light irradiation the CV of the samples in KOH can be explained considering that at the wavelength used in the experiments, at both R400 and R600 samples electrons and holes are generated. The increase

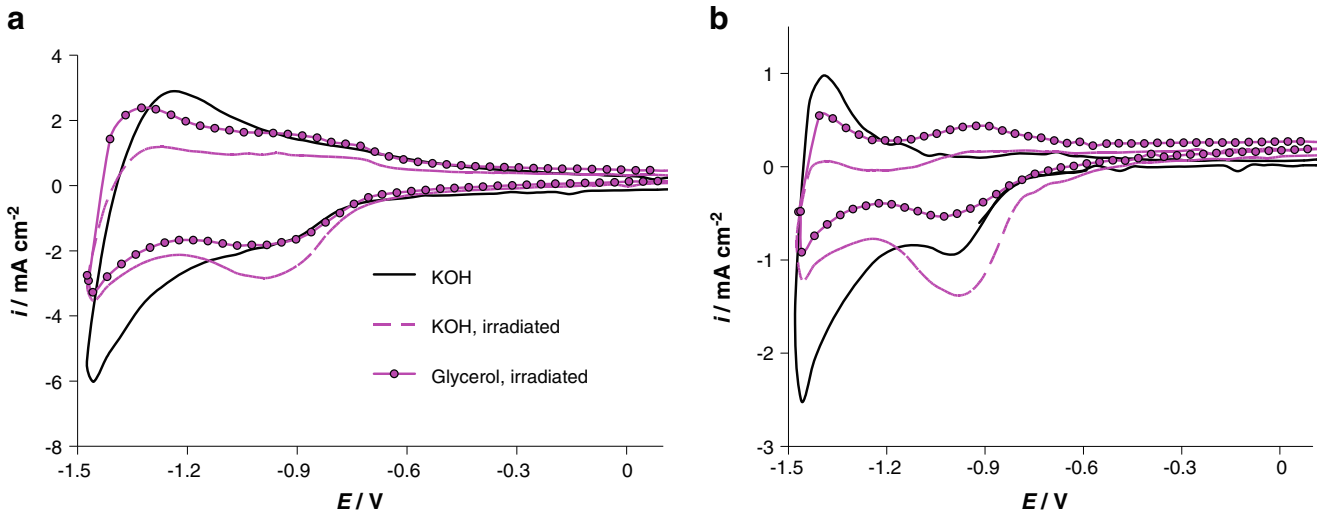

Fig. 10 Cyclic voltammograms for sample R400 (**a**) and R600 (**b**) under irradiation λ=365 nm in absence and in presence of glycerol 0.1 M, compared with the one in KOH 0.1 M in the dark

in the current peak (I) indicates that the photo-produced holes can restore T^{+4} sites for R400 and R600.

- The photo-current on set measured at R400 at potential more negative than the apparent flat band potential suggests that this current is related to the restoration of surface sites. However, the saturation current in KOH, at this electrode is lower than that measured at R600: the change of the kind of superficial sites and in turn of superficial terminations may result in a less favourable process of water oxidation. Moreover, the more positive effect of G registered at R400 can be connected to the high concentration of sites available for its adsorption at this sample.
- G is adsorbed at the superficial oxygen vacancies, preferentially with respect to OH, and it replaces OH terminations.
- The catalytic reduction of G (in the dark) is indicated to be direct or mediated by H incorporated in the lattice, at R400 and R600, respectively.
- The photo-catalytic behaviour observed confirms that G is strongly adsorbed at V_O and it hinders the restoration of V_O by photo-generated holes. The high hole scavenger character of G is also confirmed by the great increase in the photo-currents at higher positive potential. At the same time, if photo-currents in KOH and in the presence of G are compared, the higher gain in photo-current measured at R400 suggests that in any case, the most important role is played by the concentration of V_O available for G adsorption.

Conclusions

The work evidenced the importance of the defectivity of TiO_2 not only on the photo-activity of the samples (TiO_2 would not be photo-active if it was not defective), but also because it strongly affects the behaviour of G at these structures. The molecule of G resulted strongly adsorbable at V_O and this affects the behaviour of the structures and the catalysis of both reduction and photo-oxidation of G.

In particular, when a possible photo-catalytic process is thought the nature of n-type semiconductor, as well as the strong hole scavenger character of G, can be usefully exploited in order to obtain the oxidation of the molecule. Evolution of H_2, coupled as cathodic semireaction, could further increase the interest on the process.

If the reduction process is concerned, the results of the present work showed that when the concentration of V_O is rather high, the adsorbed G can react directly with the electrons injected in the system; when the concentration of V_O available for G adsorption is limited its indirect reduction seems to proceed via H incorporated in the lattice.

Further study is still on the way in order to verify these hypotheses: experiments performed in a greater electrode scale will allow to investigate on possible by-products which originate during the processes and to confirm the reaction mechanisms.

Acknowledgements The authors wish to thank MIUR and FONDAZIONE ORONZIO DENORA for financial support. PhD Giovanna Mura and PhD Elodia Musu of the Telemicroscopy Laboratory of Sardegna Ricerche are gratefully acknowledged for the SEM analysis.

References

1. Pagliaro M, Ciriminna R, Kimura H, Rossi M, Della Pina C (2007) From glycerol to value-added products. Angew Chem Int 46:4434–4440
2. Zheng Y, Chen X, Shen Y (2008) Commodity chemicals derived from glycerol, an important biorefinery feedstock. Chem Rev 108:5253–5277
3. Zhou CHC, Beltramini JN, Fan YX, Lu GQM (2008) Chemoselective catalytic conversion of glycerol as a biorenewable source to valuable commodity chemicals. Chem Soc Rev 37:527–549
4. Alvarez MG, Segarra AM, Contreras S, Sueiras JE, Medina F, Figueras F (2010) Enhanced use of renewable resources: transesterification of glycerol catalyzed by hydrotalcite-like compounds. Chem Eng J 161:340–345
5. Miller H (2000) Major fiber producers hop on corterra bandwagon. Int Fiber J 15:14–16
6. Rudie R (2000) Cargill dow sows seeds of future fibers; will build $ 300 million PLA polymer plant. Int Fiber J 15:8–12
7. Dasari M, Kiatsimkul P, Sutterlin W, Suppes GJ (2005) Low-pressure hydrogenolysis of glycerol to propylene glycol. Appl Catal A 281:225–231
8. Augugliaro V, Hamed El Nazer HA, Loddo V, Mele A, Palmisano G, Palmisano L, Yurdakal S (2010) Partial photocatalytic oxidation of glycerol in TiO_2 water suspensions. Cat Today 151:21–28
9. Daskalaki VM, Panagiotopoulou P, Kondarides DI (2011) Production of peroxide species in Pt/TiO_2 suspensions under conditions of photocatalytic water splitting and glycerol photoreforming. Chem Eng J 170:433–439
10. Palmas S, Polcaro AM, Rodriguez Ruiz J, Da Pozzo A, Mascia M, Vacca A (2010) TiO_2 photoanodes for electrically enhanced water splitting. Int J Hydrogen Energy 35:6561–6570
11. Mura F, Masci A, Pasquali M, Pozio A (2010) Stable TiO_2 nanotubes arrays with high UV photoconversion efficiency. Electrochim Acta 55:2246–2251
12. Macak JM, Zlamal M, Krysa J, Schmuki P (2007) Self-organized TiO_2 nanotube layers as highly efficient photocatalysts. Small 3:300–304
13. Zwilling V, Aucouturier M, Darque-Ceretti E (1999) Anodic oxidation of titanium and TA6V alloy in chromic media. An electrochemical approach. Electrochim Acta 45:921–929
14. Khan MA, Jung HT, Yang OB (2006) Synthesis and characterization of ultrahigh crystalline TiO_2 nanotubes. J Phys Chem B 110:6626–6630
15. Chen YS, Crittenden JC, Hackney S, Sutter L, Hand DW (2005) Preparation of a novel TiO_2-based p-n junction nanotube photocatalyst. Environ Sci Technol 39:1201–1208
16. Xue W, Zhang G, Xu X, Yang X, Liu C, Xu Y (2011) Preparation of titania nanotubes doped with cerium and their photocatalytic activity for glyphosate. Chem Eng J 167:397–402
17. Mohapatra SK, Raja KS, Mahajan VK, Misra M (2008) Efficient photoelectrolysis of water using TiO_2 nanotube arrays by minimizing recombination losses with organic additives. J Phys Chem C 112:11007–11012

18. Yu J, Hai Y, Jaroniec M (2011) Photocatalytic hydrogen production over CuO-modified titania. J Colloid Interface Sci 357:223–228
19. Palmas S, Da Pozzo A, Mascia M, Vacca A, Nova I, Matarrese R (2011) Effect of the preparation conditions on the performance of TiO_2 nanotube arrays obtained by electrochemical oxidation. Int J Hydrogen Energy 36:8894–8901
20. Nowotny J, Bak T, Nowotny MK, Sheppard LR (2007) Titanium dioxide for solar-hydrogen IV. Collective and local factors in photoreactivity. Int J Hydrogen Energy 32:2651–2659
21. Kim DJ, Pyun SI, Yoon YG (1996) Determination of energy distribution of donor levels in anodically passivating TiO_2 film. J Alloys Compd 235:182–187
22. Muñoz AG (2007) Semiconducting properties of self-organized TiO_2 nanotubes. Electrochim Acta 52:4167–4176
23. Muñoz AG, Chen Q, Schmuki P (2007) Interfacial properties of self-organized TiO_2 nanotubes studied by impedance spectroscopy. J Solid State Electrochem 11:1077–1084
24. Bolts JM, Wrighton MS (1976) Correlation of photocurrent-voltage curves with flat-band potential for stable photoelectrodes for the photoelectrolysis of water. J Phys Chem 80:2641–2645
25. Beermann N, Boschloo GK, Hagfeldt A (2002) Trapping of electrons in nanostructured TiO_2 studied by photocurrent transients. J Photochem Photobiol A 152:213–218
26. Henderson MA (1996) Structural sensitivity in the dissociation of water on TiO_2 single-crystal surfaces. Langmuir 12:5093–5098
27. Bezrodna T, Puchkovska G, Shymanovska V, Baran J, Ratajczak H (2004) IR-analysis of H-bonded H_2O on the pure TiO_2 surface. J Mol Struct 700:175–181
28. Bredow T, Jug K (1995) Theoretical investigation of water adsorption at rutile and anatase surfaces. Surf Sci 327:398–40
29. Cappelletti G, Ricci C, Ardizzone S, Parola C, Anedda A (2005) Aged titania nanoparticles: the simultaneous control of local and long-range properties. J Phys Chem B 109:4448–4454